



Supplementary Materials for

Polymerization in the Actin ATPase clan regulates hexokinase activity in yeast.

Patrick R Stoddard, Eric M. Lynch, Daniel P. Farrell, Annie M. Dosey, Frank DiMaio, Tom A. Williams, Justin M. Kollman, Andrew W. Murray*, Ethan C. Garner*

* co-corresponding authors.

Correspondence to: awm@mcb.harvard.edu (AWM) and egarner@g.harvard.edu (ECG).

This PDF file includes:

Materials and Methods
Figs. S1 to S20
Tables S1 to S4
Captions for Movies S1 and S2
References 29 - 60

Other Supplementary Materials for this manuscript includes the following:

Movies S1 and S2 available on the Science website
The complete treefile used to create Figure 3B available on the Science website
A high-resolution version of Table S3 available on the Science website

Materials and Methods

Strains and Culture Conditions

Unless otherwise noted, *S. cerevisiae* was grown at 30 °C in CSM supplemented with the appropriate carbon sources. For viability/plating assays, yeast were grown in citrate buffered synthetic medium (CBS) (25) with appropriate carbon source.

Plasmid Construction and Cloning

Table S4 lists strains and plasmids used in this study. Constructs for the transformation of *S. cerevisiae* were generated by fusion PCR (29), and the cells were transformed with purified PCR products (30). Clones were verified by amplification of the genomic locus followed by Sanger sequencing of the purified product.

Proteins were tagged with fluorescent proteins as C-terminal fusions using an 8 amino acid linker (GDGAGLIN).

For protein overexpression and purification from *E. coli*, glucokinases/hexokinases were cloned as his₆SUMO fusion constructs (31) into T7 plasmids by Gibson assembly (32). The plasmids were purified, and their sequences confirmed by Sanger sequencing using universal primers.

Media Transitions

Cells from cultures grown to saturation were loaded into a microfluidic cell (CellAsic), and their spent medium flowed over them. Cells were exchanged into fresh media containing 2 % glucose. Media was pumped at 2 PSI.

Microscopy

Images were taken on a Nikon Ti inverted microscope with a Yokogawa spinning disc confocal unit, 447, 488, 515, and 595 nm lasers, a Hamamatsu Orca camera operated with MetaMorph software. 8 μm z-stacks were taken in 0.2 μm increments. Z-stacks were converted to 8-bit, maximum intensity projection images, and contrast adjusted in ImageJ (33).

The filament disassembly video (Movie S2) was taken using Nikon Ti-E inverted microscope (Nikon) equipped with a 60× objective (PlanApo, numerical aperture 1.4, oil), GFP filter (Chroma Technology), and a CoolSNAP charge-coupled device camera (Photometrics) using streaming acquisition of a single focal plane.

Protein Purification

BL21(DE3) Rosetta containing the his₆SUMO fusion plasmid were grown to OD₆₀₀ ~ 0.6 and induced overnight with 0.4 mM IPTG at 16 °C. His₆SUMO fusion products were purified and cleaved as in (31). Proteins were further purified and exchanged into HKM-buffer (20 mM HEPES-KOH pH 7.5, 100 mM KCl, 1 mM MgCl₂, 10 % glycerol (v/v), 10 mM β-mercaptoethanol) using an S200 16/600 column on an AKTA FPLC. Fractions were pooled and concentrated. Aliquots were snap frozen in liquid nitrogen and stored at -80°C until needed.

Ultracentrifugation

Unless otherwise noted, polymerization reactions were done in HKM-buffer and contained 5 μM enzyme, 10 mM glucose, and 10 mM MgATP. Polymerization reactions were spun in a TLA-100 (Beckman) at 100k rpm for 30 minutes at 30 °C. Supernatants were removed and added to

equal volume of 2xSDS-Buffer. Pellets were resuspended by heating at 65 °C in 2 volumes of 1xSDS-Buffer. Fractions were subjected to SDS-PAGE, stained with Coomassie Blue G250, and band intensities were quantified in imageJ (33).

Light Scattering

Polymerization reactions were initiated by mixing 15 μM Glk1 with an equal volume of 10 mM glucose and 10 mM MgATP or 10 mM glucose-6-phosphate and 10 mM MgADP using a SFA-20 rapid mixer (Hi-Tech Scientific), driven by a pneumatic drive unit (Hi-Tech Scientific). The 90-degree scattering of the solution at 315nm was measured using a Fluorolog-3 (Horiba).

Crystallization, Diffraction, and Refinement

Glk1 was exchanged into 5 mM HEPES-KOH pH 7.5, 20 mM KCl, 1 mM MgCl₂, 0.5 mM TCEP and concentrated to 11 mg/mL by centrifugal ultrafiltration (Amicon Ultra; Millipore). Conditions were screened around the conditions used in (9) as hanging drops. Final crystallization conditions were 2.4 M (NH₄)₂HPO₄, 0.1 M CHES pH 9.4 (2:1 protein:well-solution) with crystals forming after 5 days at 20 °C. Crystals were cryoprotected by briefly soaking in well solution supplemented with 18 % glycerol before freezing.

X-ray data were collected at the Advance Photon Source beamline 24-ID-C at the Argonne National Laboratory. 180° of data was collected with a 10 μm beam at 20 % transmission. Reflection data were indexed, integrated, and scaled with HKL2000 (34). Initial phases were obtained using Phaser (35) for molecular replacement, using the *S. cerevisiae* hexokinase-2 structure (PDB ID: 1IG8) (19) as a search model. The model was built in Coot (36) and refined using Phenix.refine (37). Positional and B-factor refinement with TLS, torsion angle, and NCS restraints were used. Phosphates from the crystallization condition were modeled into densities of appropriate size that were coordinated by basic and polar residues. The asymmetric unit of the crystal contained six protein chains. Residues 51-59 were omitted from all chains because this loop had poor density. Besides this omission, chains A, C, and F contain residues 1-500, chains B and E contain residues 3-500, chain D contains residues 4-500. Chain A was used for analysis and generation of figures.

CryoEM sample preparation and data collection

Glk1 was buffer-exchanged into 20 mM K-HEPES pH 7.5, 100 mM KCl, 1mM MgCl₂, and 0.5 mM DTT using a ZebaSpin 7K MWCO desalting column. Glk1 filaments were then formed by incubating 20 μM Glk1 with 10 mM glucose, 10 mM MgCl₂, and 10 mM ATP for 20 minutes at room temperature. CFLAT2/2 holey-carbon grids (Protochips Inc.) were glow-discharged using a PELCO easiGlow on the negative setting, with a current of 20 mA for 20 seconds at 0.39 mBar in air. To prepare samples for cryoEM, 2.5 μl Glk1 filament sample (20 μM) was applied to glow-discharged grids and blotted away 4 times successively, before being plunged into liquid ethane using a Vitrobot (FEI co.). The first 3 blots were performed manually by immediately touching Whatman Grade 1 filter paper to the edge of the grid to rapidly wick away solution (outside of the Vitrobot), with the final blot performed on the Vitrobot with standard filter paper (Ø55/20mm, Grade 595). The Vitrobot was set to room temperature and 100% humidity, with blot force, wait time, drain time, and offset all set to 0. Data was collected on a Titan Krios (FEI co.) with a Quantum GIF energy filter (Gatan Inc.) operating in zero-loss mode with a 20 eV slit width. Movies were acquired on a K-2 Summit Direct Detect camera, operating in super-resolution mode

with a pixel size of 0.525 Å/pixel, with 50 frames and a total dose of 90 electrons/Å². Leginon software was used for automated data collection (38).

CryoEM data processing

Movie frames were aligned, dose-weighted, and binned 2X using MotionCor2 (39), and CTF parameters were estimated using GCTF (40). Subsequent cryoEM processing steps are summarized in Figure S12. Helices were picked manually from a subset of images using Relion (41), exported to cryoSPARC (42), and used to generate initial 2D classes which were then used as templates for picking from all micrographs in cryoSPARC. Further 2D classification (4 rounds) was performed in cryoSPARC, and particles from good classes showing high-resolution features were exported to Relion. Relion 3D refinement produced a structure at 5.8Å resolution, and further masked refinement produced a structure at 3.9Å. The mask encompassed 4 subunits, and was used in all subsequent steps. Relion 3D classification was then performed, and particles contributing to the class with the highest resolution were selected for further refinement. In order to formally impose helical symmetry, initial estimates of helical symmetry were obtained by rigid body fitting of the Glk1 crystal structure into the 3.9Å cryoEM map, then measuring the translation and rotation between adjacent subunits in Chimera (43). These estimates (rise 59.9Å, rotation 119.7 degrees) were used as starting values for Relion 3D refinement with helical symmetry search, and the resulting refined helical symmetry values (rise 60.1Å, rotation 120.4 degrees) were then imposed in a final Relion 3D refinement. The final map was sharpened using Relion post-processing, and resolution was estimated at 3.8Å using the FSC_{0.143} cutoff. Details of 3D reconstructions are summarized in Table S2.

Atomic model refinement

The Glk1 filament model was based on the solved crystal structure, PDB ID: 6P4X. First, small gaps in the model were resolved with RosettaCM (44) which used the model as a template and the cryoEM map EMD-20309 as a guide. Due to low convergence, residues 47-64 were removed, and completed with RosettaES (45). Next, the model was further refined using the density and fragment sampling as described in (46). Finally, all-atom refinement was performed in Cartesian space utilizing the Rosetta FastRelax (47) protocol. Model to map validation data was generated using phenix (37), and the Rosetta density_tools application (46).

Homolog Selection

Glucokinase and hexokinase homologs for purification and polymerization testing were found by reciprocal BLAST (48) searches and were informed by synteny when possible. Protein alignments of the tested enzymes were made using Clustal Omega (49).

Actin superfamily fold similarities

Our analyses were based on a dataset of HMMs representing each member of the actin fold family obtained from the Pfam database (version 32.0). For families in which the N and C terminal domain halves were represented by different Pfam HMMs (hexokinase, glucokinase, and hydantoinase), we built new HMMs by searching the full-length query sequence of *S. cerevisiae* Glk1 (UniProtKB – P17709) for the hexokinases, the *E. coli* Glk (UniProtKB – P0A6V8) for the glucokinases, and the *E. coli* HyuA (UniProtKB – Q46806) for the hydantoinases against the UniProtKB database using Jackhmmer (50). Pairwise similarity comparisons between the HMMs were performed using HHsearch from the HH-Suite 3

package (51).

Actin fold phylogeny

The phylogeny was based on a set of sequences assembled previously (4), but updated to include the full set of folds analyzed here. Representative sequences for each fold were selected by CD-HIT (52) clustering of the highly redundant set of sequences used to construct the corresponding HMMs. Sequences were aligned using the L-INS-i mode in mafft (53), poorly aligning regions of the alignment were identified and removed using the "gappyout" mode in trimAl (54), and the phylogeny was inferred under the LG+C20+F model in IQ-Tree 1.6.10 (28). Bootstrap supports were computed using the UFBoot2 algorithm (55).

Glucokinase Activity Assays

Glucose-6-phosphate production was measured in HKM-buffer at 30 °C. Timepoints were quenched in an equal volume of 100 mM EDTA at 95 °C. Glucose-6-phosphate concentration was measured in each timepoint by a colorimetric enzyme-coupled reaction as in (56).

Competition Experiments

Strains were grown overnight in CSM with the appropriate carbon source, diluted into fresh medium and grown to mid exponential phase. mCherry labeled wild-type cells were mixed with GFP labeled strains in equal numbers. Cells were back diluted 200-fold every 48 hours, and samples taken two hours later. The ratio of the two strains was measured by flow cytometry (Fortessa) and the data analyzed in FlowJo (Beckton and Dickinson).

Viability Experiments

Strains were conditioned in CBS/Galactose for 48 hours, being diluted to 1×10^5 cells/mL in fresh medium every 12 hours. Cells were harvested, washed twice in CBS with no carbon source, and plated onto either CBS/glucose or CBS/galactose. Colonies were counted after three days at 30 °C.

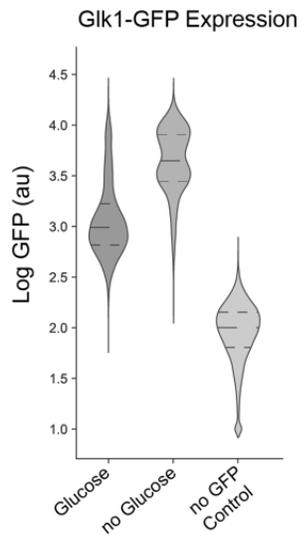


Fig. S1 - Glk1 expression under different growth conditions.

Green fluorescence of cells expressing Glk1-msfGFP from the Glk1 locus were measured by flow cytometry while growing in glucose or 12 hours after glucose was depleted from the culture (*no Glucose*). Middle line in each violin represents the median of the distribution. Upper and lower lines represent top and bottom quartiles. Glk1 expression increases in the absence of glucose. The no GFP Control shows the green autofluorescence of *S. cerevisiae*.

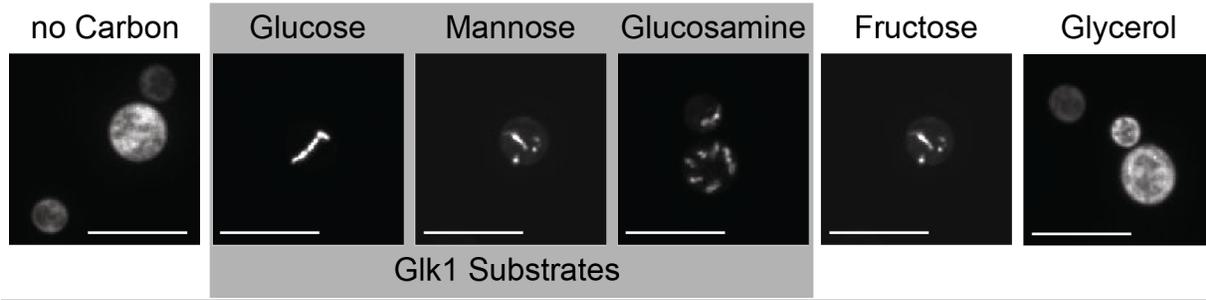


Fig. S2 - Glk1-msfGFP polymerizes in cells in response to several sugars.

Maximum intensity projections of confocal z-stacks of Glk1-msfGFP cells. Cells were grown to saturation and washed in media containing no carbon. Cells were refeed the sugar indicated, and fluorescence micrographs were taken 1 minute after refeeding. Carbon sources that are Glk1 substrates are boxed in gray. Scale bar: 10 μ m.

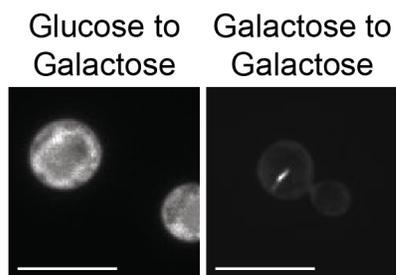


Fig. S3 - Galactose triggers Glk1-msfGFP polymerization only in galactose conditioned cells.

Fluorescence micrographs of cells expressing Glk1-msfGFP. Cells were either grown to saturation in glucose-containing medium or galactose containing medium. Glk1-msfGFP polymerizes in galactose conditioned cells when refed galactose but not in glucose conditioned cells. This is likely due to the suppression of the galactose transporter (Gal2) and galactokinase (Gal1) by the presence of glucose (57). Scale bar: 10 μ m.

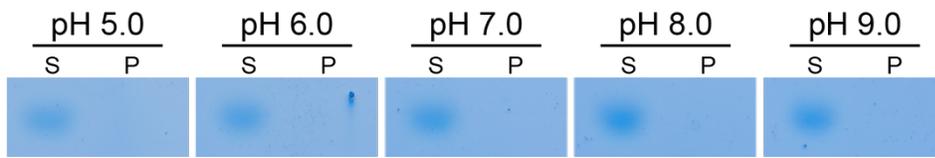


Fig. S4 - Glk1 does not polymerize in response to change in pH.

10 μ M Glk1 was ultracentrifuged at pH values from 5.0 to 9.0, and the supernatant (S, *left*) and pellet (P, *right*) were subjected to SDS-PAGE and stained with Coomassie blue.

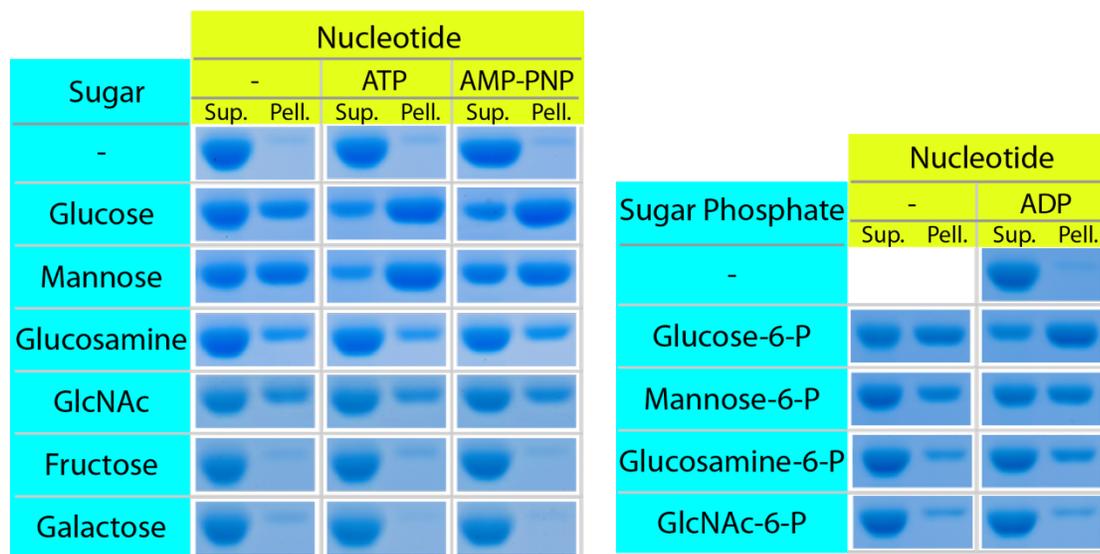


Fig. S5 - Glk1 polymerization in the presence of different ligands.

Purified Glk1 was ultracentrifuged in the presence of different ligand combinations. The supernatant (*left*) and pellet (*right*) of each condition were subjected to SDS-PAGE. Glk1 polymerizes in response to its substrates (glucose, mannose, and glucosamine), inhibitors (GlcNAc and GlcNAc-6-P), and products (glucose-6-P, mannose-6-P, and glucosamine-6-P), but not to other sugars (fructose and galactose).

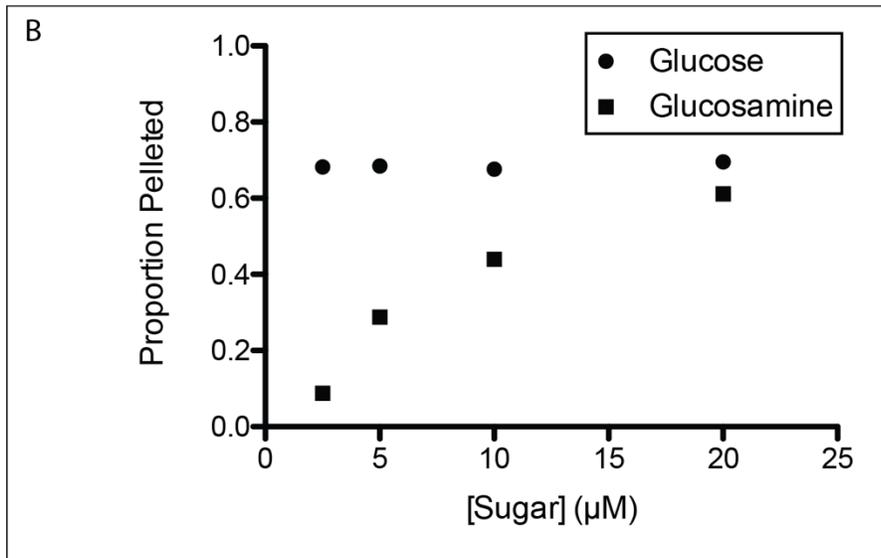
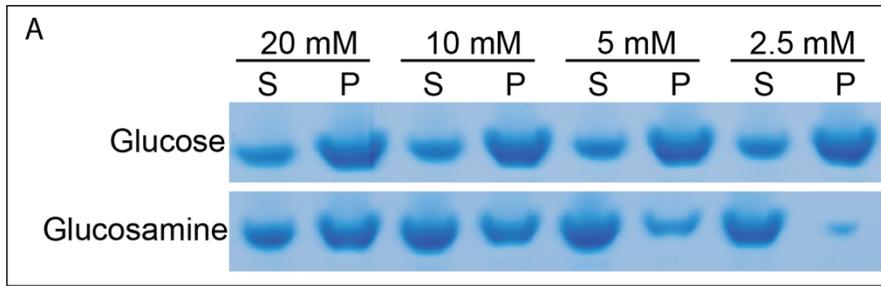


Fig. S6 - The difference in Glk1 pelleting efficiency with different ligands is from different ligand affinities. $6\mu\text{M}$ Glk1 with 10mM ATP and varied glucose and glucosamine concentration were spun at $436k \times g$ for 30 min at 30°C . The pellet and supernatant were subjected to SDS-PAGE and stained with Coomassie blue G250 (A). Quantification of the supernatant and pellet band at each concentration reveals that as glucosamine concentration increases, the amount of Glk1 in polymer approaches the amount in polymer in glucose (B).

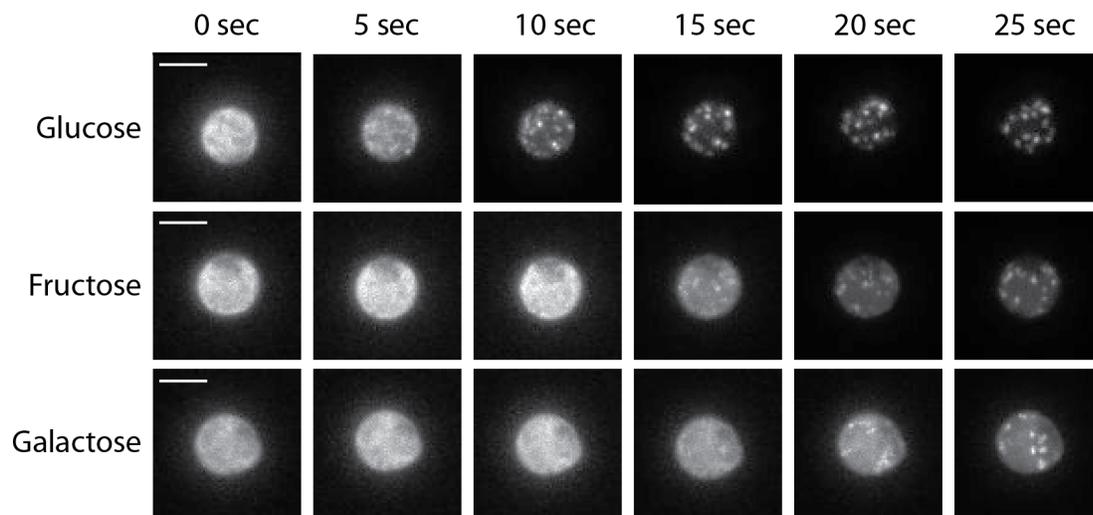


Fig. S7 - Refeeding sugars that are not Glk1 substrates results in slower Glk1-msfGFP polymerization than refeeding glucose. Glk1-msfGFP cells grown to saturation on glucose (*top and middle*) or galactose (*bottom*) were refeed glucose (*top*), fructose (*middle*), or galactose (*bottom*). Glucose caused polymerization more rapidly than either fructose or galactose. This is consistent with fructose and galactose causing polymerization in vivo by accumulation of glucose-6-phosphate. Scale bar: 5 μ m.

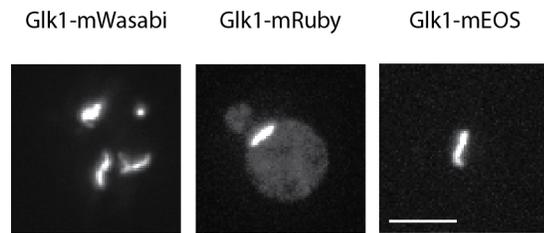


Fig. S8 - Glk1 polymers look similar when other fluorescent tags are used.

Fluorescence micrographs of cells expressing Glk1-mWasabi (left), Glk1-mRuby (center), and Glk1-mEOS (right). Cells were grown to saturation and reintroduced to glucose before imaging. Scale bar: 5 μm .

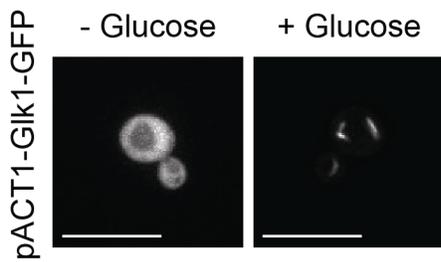


Fig. S9 - Fluorescence micrographs of cells expressing Glk1-msfGFP under the Actin promoter.

Cells were harvested growing exponentially on glucose and imaged in the absence of glucose (*left*) or in the presence of glucose (*right*). Strong, constitutive expression of Glk1-msfGFP divorces cell state from polymer presence. Scale bar: 10 μm .

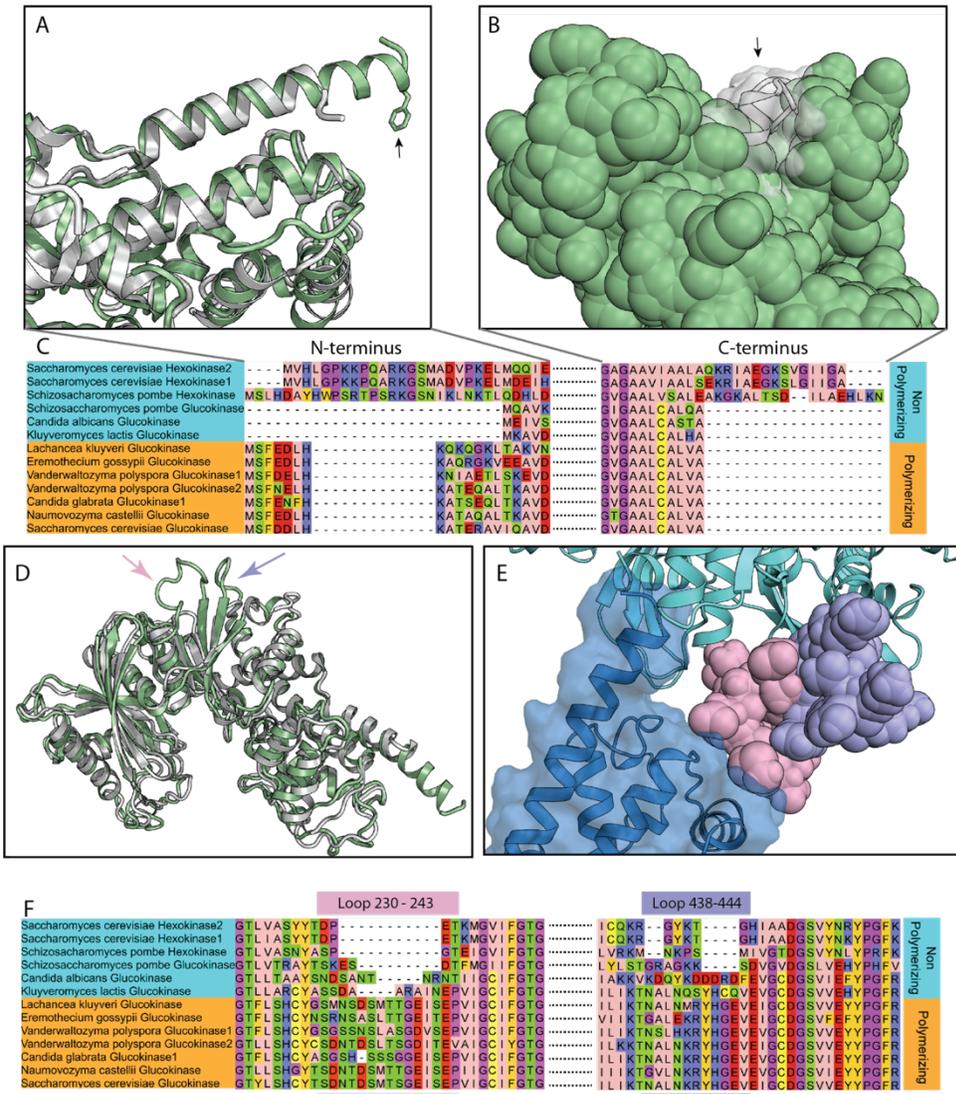


Fig. S10 - Residues involved in Glk1 filament contacts are conserved amongst polymerizing glucokinases but not amongst non-polymerizing glucokinases or hexokinases.

A) Comparison of the N-terminus of Hxk2 (*white*, PDB ID: 1IG8) and Glk1 (*green*). The N-terminal helix of Glk1 extends beyond the body of the protein, while the N-terminal helix of Hxk2 ends flush to the body. Glk1's helix contains a solvent exposed phenylalanine. **B)** Models of Hxk2 and Glk1 show that the C-terminal helix of Hxk2 (*white ribbon/transparent surface*) extends beyond that of Glk1 (*green spheres*). This means that Hxk2 does not have the hydrophobic pocket involved in Glk1 polymerization. **C)** Alignment of all tested enzymes. The N terminus (MSF(e/d)(e/d)LHK) and C-terminus (LCALVA) are conserved amongst enzymes that polymerize and divergent amongst enzymes that do not. **D)** The loop from Glk1 residue 230-243 (*pink arrow*), and Glk1 residue 438-444 (*purple arrow*) are larger than their corresponding loops in Hxk2 (*white*). **E)** Close up of longitudinal interface between two subunits in a model of a Glk1 filament. Loop 230-243 (*pink spheres*) contacts the next subunit (*blue ribbon and surface*), and loop 438-444 (*purple spheres*) packs tightly against loop 230-243. **F)** Alignment of

all tested enzymes in loop regions. Both loops are extended in all polymerizing enzymes and are truncated or divergent in non-polymerizing enzymes.

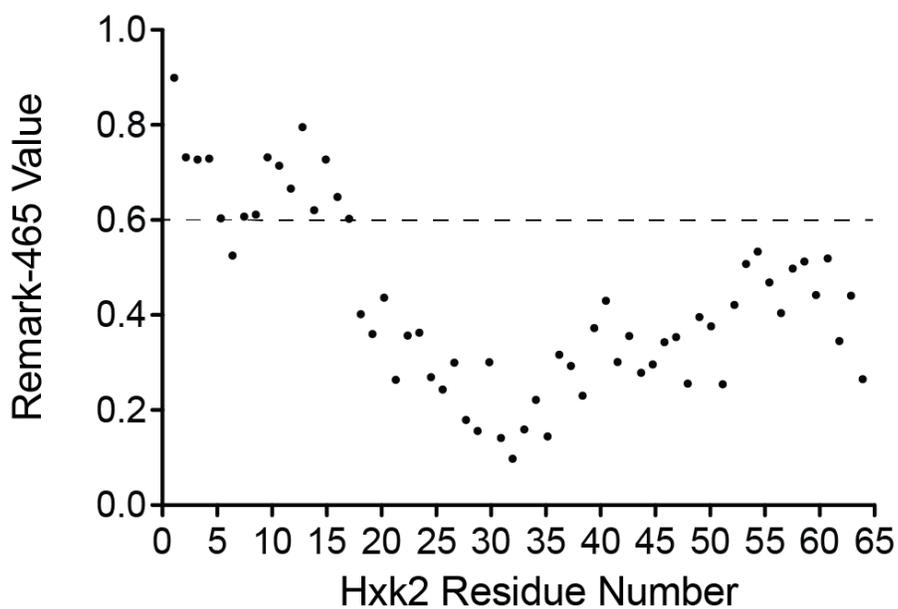


Fig. S11 - The unmodeled residues in the Hxk2 crystal structure are likely disordered.

The Remark-465 values of the first 65 residues of Hxk2. Values above 0.6 are more likely to be disordered. The first 16 residues are not modeled in the Hxk2 crystal structure (PDB ID: 1IG8), and this region is predicted to be disordered.

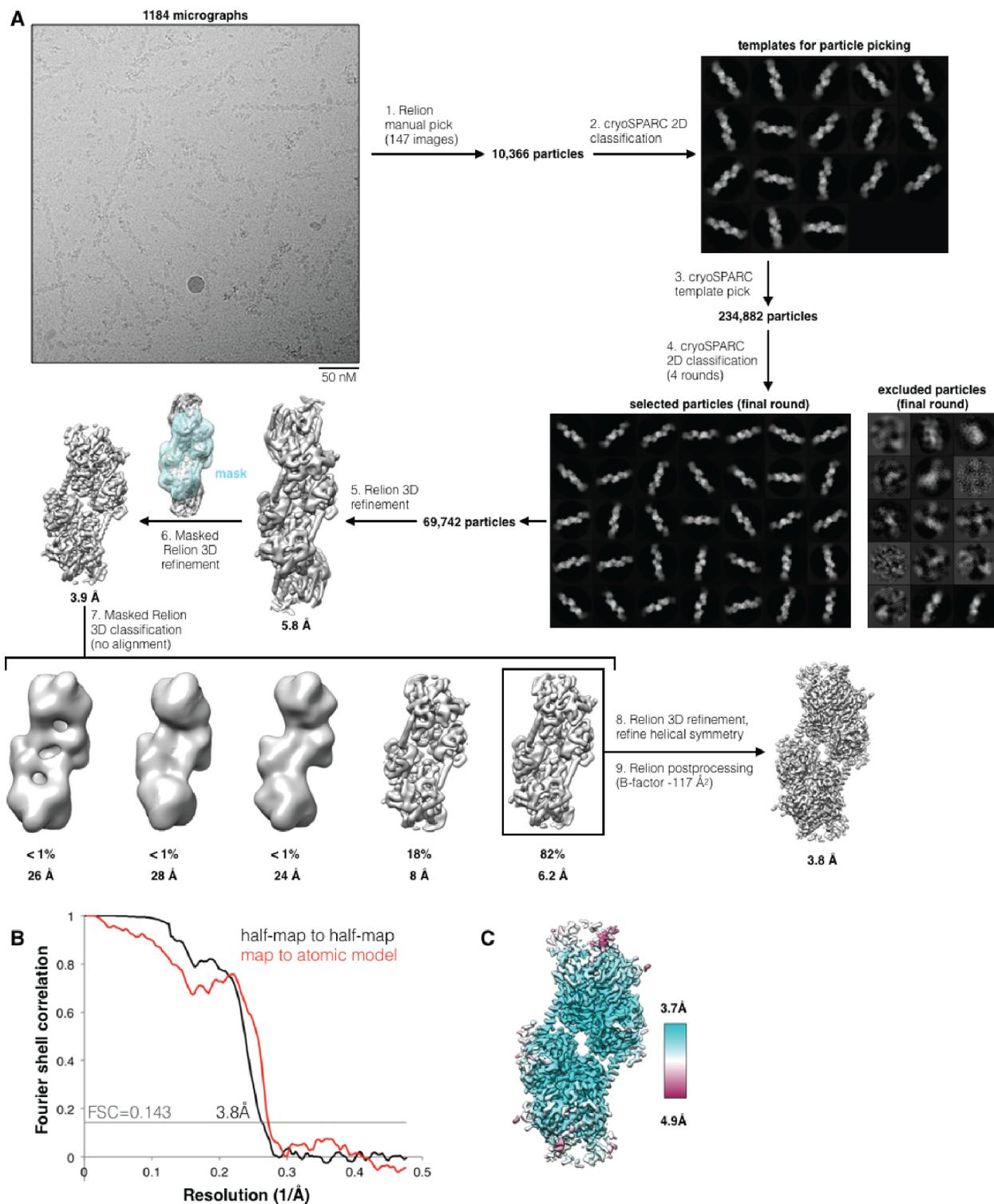


Fig. S12 - CryoEM data processing and structure validation. (A) Flowchart of cryoEM data processing. Additional details are provided in the Methods section. (B) Half-map to half-map and map to atomic model FSC curves for the Glk1 filament structure. (C) Relion local resolution estimate of the Glk1 filament structure, showing a local resolution range of 3.7-4.9 Å.

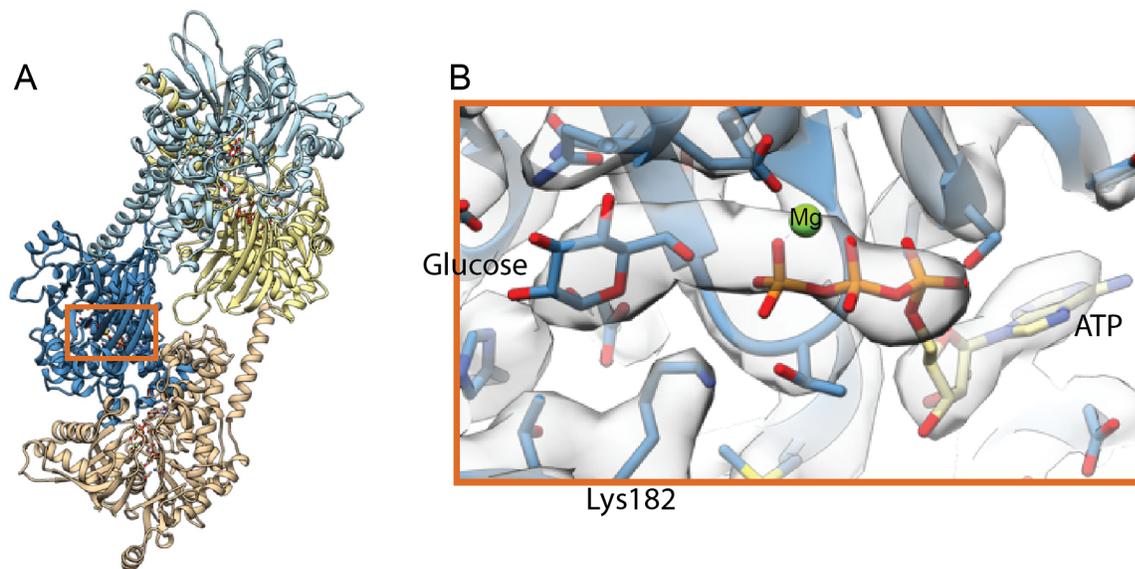


Fig. S13 - Glk1 filaments have magnesium and glucose and ATP or G6P and ADP bound in their active site.

A) Cartoon representation of four subunits within a Glk1 filament showing where glucose and ATP are modeled within the filament. The orange box indicates the location of the ligands shown in B. **B)** Ligand density (*gray surface*) is present in the cryoEM Glk1 filament electron density. Glucose and ATP vs G6P and ADP cannot be distinguished at this resolution. Here we have modeled glucose and ATP. The catalytic lysine (Lys182) can be seen coordinating the -OH on the 6-carbon of glucose and the -OH on the gamma-phosphate of ATP.

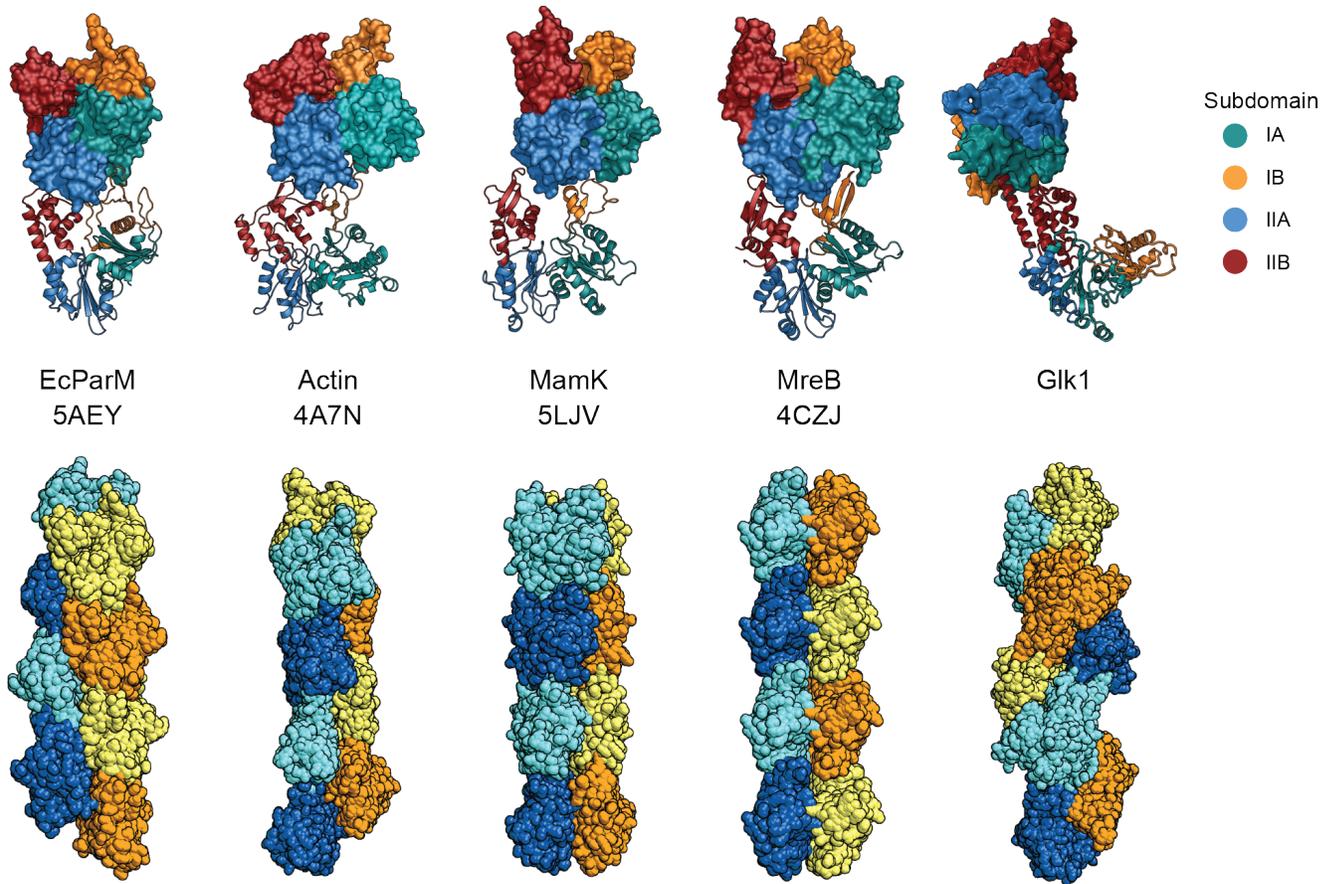


Fig. S14 - Intersubunit geometry conserved in other actin-related filaments is not present in Glk1 filaments.

Top: Amongst all other actin-related filaments, along a single strand, subdomain IB and IIB contact subdomain IA and IIA respectively. In Glk1 filaments, subdomain IIB contacts subdomain IA (5, 58-60). The top subunit is represented as a surface while the bottom subunit is represented as a ribbon.

Bottom: Despite the conserved geometry along strands in the cytoskeletal polymers, filaments are still able to achieve a variety of structures through varying subunit shape and lateral interactions.

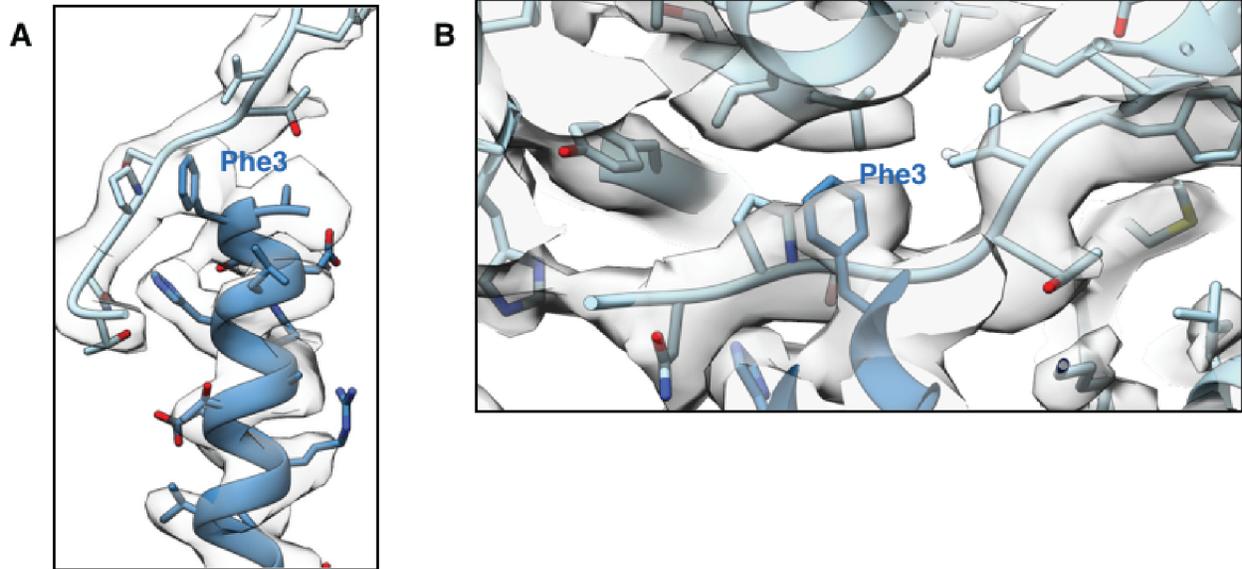


Fig. S15 - CryoEM map at the longitudinal filament interface. (A) Isolated density for the N-terminal helix at the longitudinal filament interface. (B) cryoEM map around the Phe3 binding pocket.

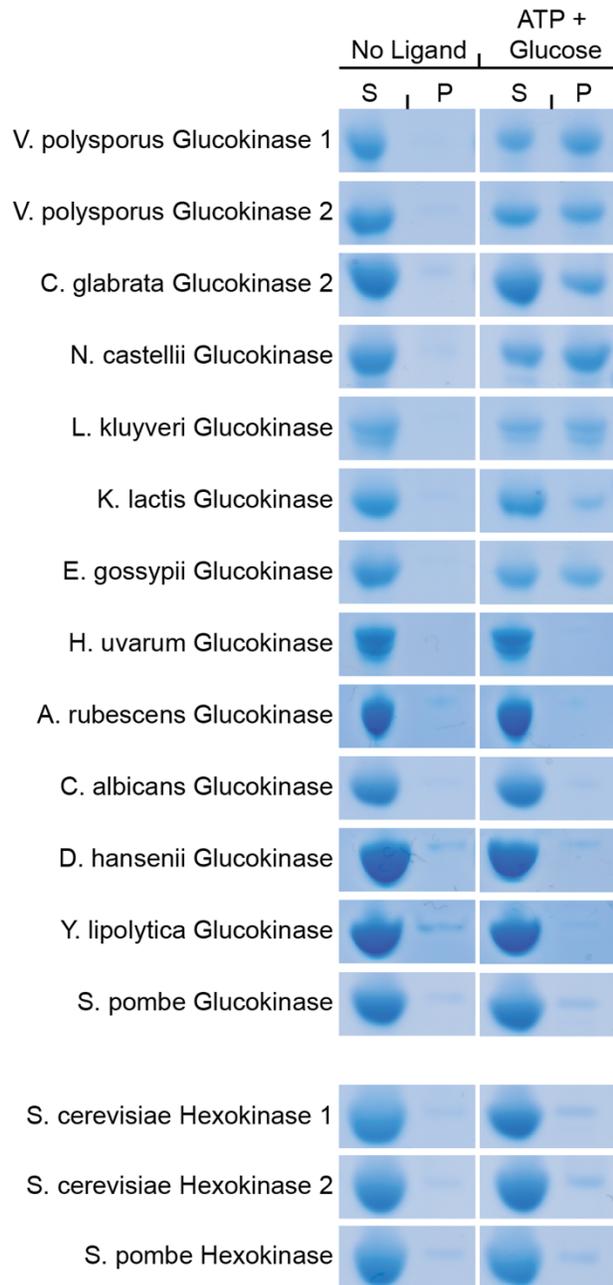


Fig. S16 - Polymerization of Glk1 homologs.

Purified Glk1 homologs (glucokinases) and Hxk1/2 homologs (hexokinases) were ultracentrifuged in the absence of ligand (*left*) or the presence of glucose and ATP (*right*). The supernatant (*S, left*) and pellet (*P, right*) were subjected to SDS-PAGE and stained with Coomassie blue. Some other glucokinases polymerize in the presence of glucose and ATP while hexokinases do not.

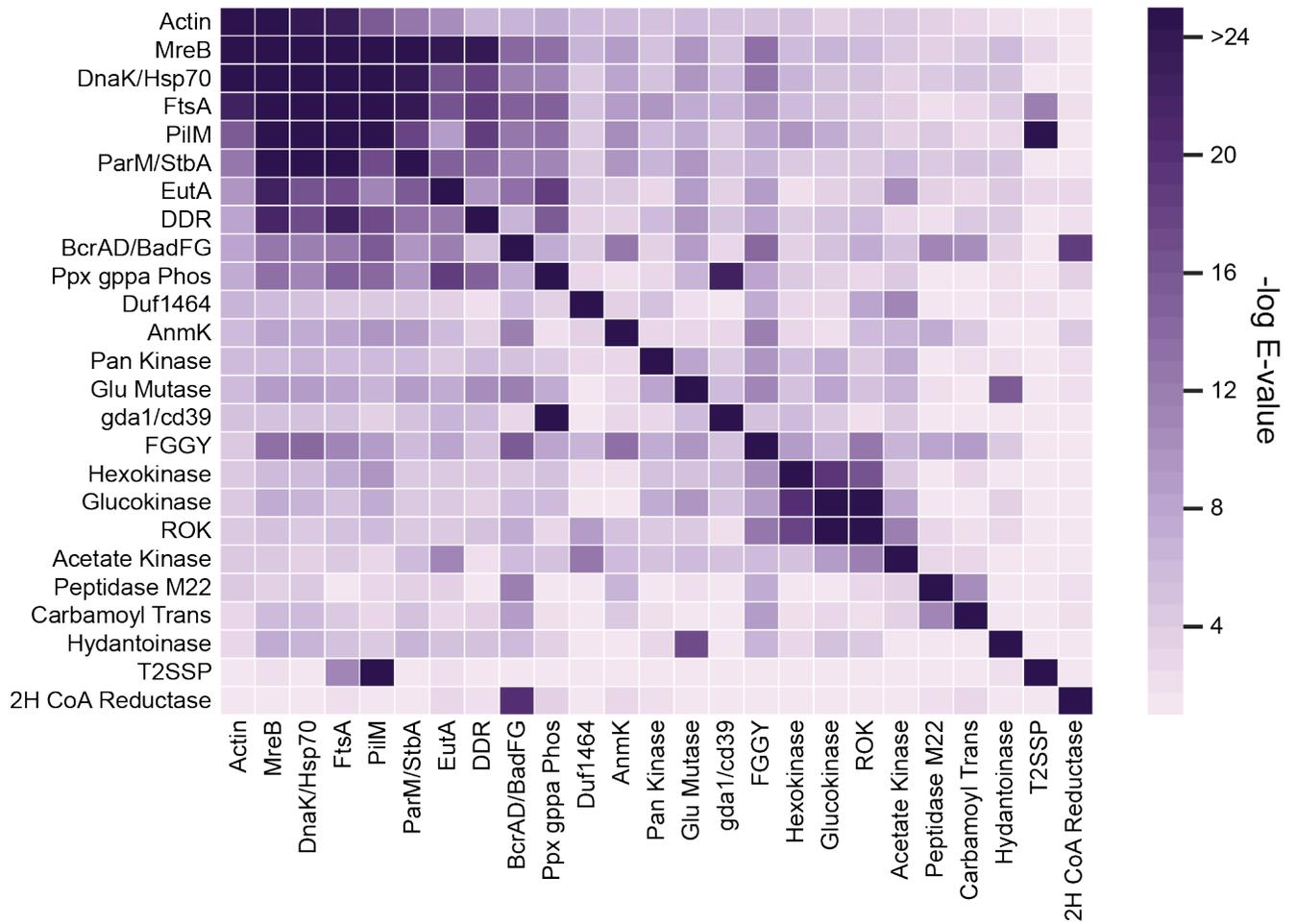


Fig. S17 - Heatmap representing the e-value for the comparison of HMM for each protein family in the Actin ATPase clan.

The values are reported as negative log of the e-value. Note that Glk1 is in the hexokinase family, not the glucokinase family in this classification.

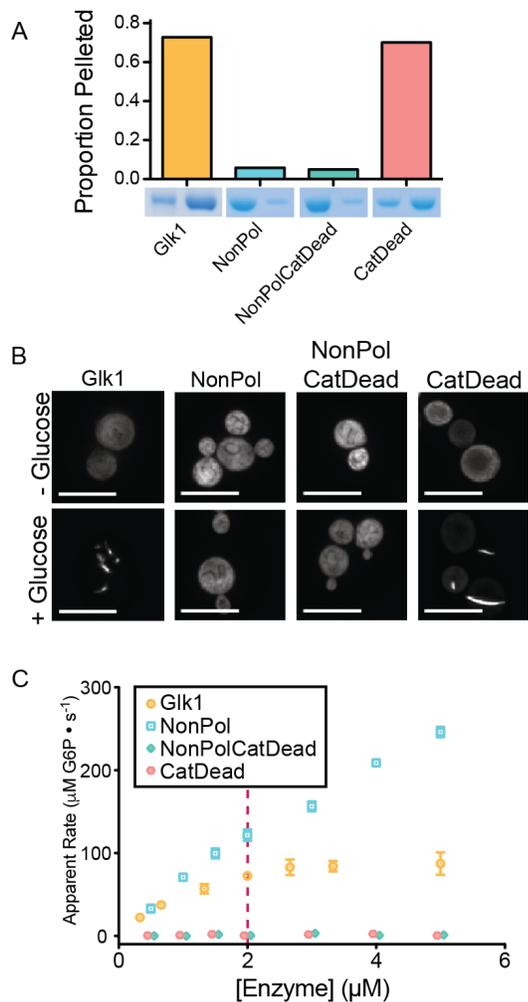


Fig. S18 - Behavior of Glk1 Mutants: (A) 5 μM purified NonPol-Glk1, NonPolCatDead-Glk1, and CatDead-Glk1 were ultracentrifuged with saturating glucose and ATP. The supernatant (*left*) and pellet (*right*) were subjected to SDS-PAGE and quantified. (B) Fluorescence images of: Glk1-msfGFP (*left*), NonPol-Glk1-msfGFP (*middle-left*), NonPolCatDead-Glk1-msfGFP (*middle-right*), or CatDead-Glk1-msfGFP (*right*) in stationary phase cells before (*top*) or after (*bottom*) refeeding glucose. Scale bar: 10 μm . (C) The rate of G6P production at different concentrations of purified Glk1, NonPol-Glk1, NonPolCatDead-Glk1, and CatDead-Glk1. Glk1's apparent rate does not increase beyond Glk1's CC (dashed line). Mean \pm SD (N = 3).

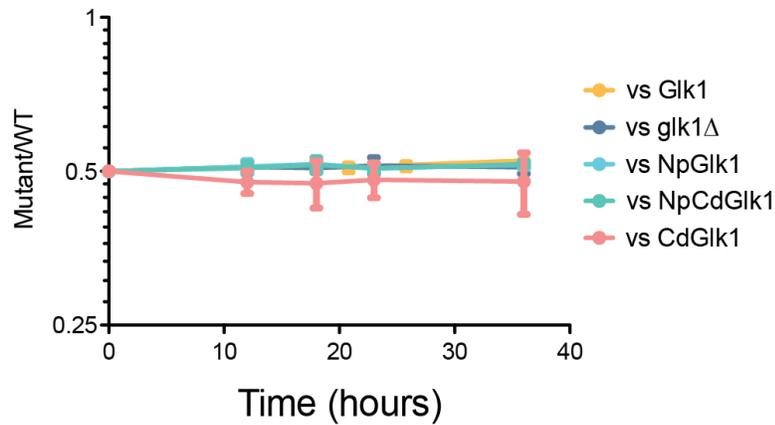


Fig. S19 - Glk1 Mutants have no fitness effect during exponential growth on glucose. Wild-type W303 labeled with mCherry were grown in competition with green labeled W303 (wild-type, *glk1Δ*, NonPol-Glk1, NonPolCatDead-Glk1, CatDead-Glk1) in CSM-Glucose. Cultures were held at low cell density by repeated back dilution to ensure continuous fermentative, log-phase growth. In these conditions, none of the Glk1 mutants or the deletion of GLK1 yielded any significant growth effect. Mean \pm SD (N = 5).

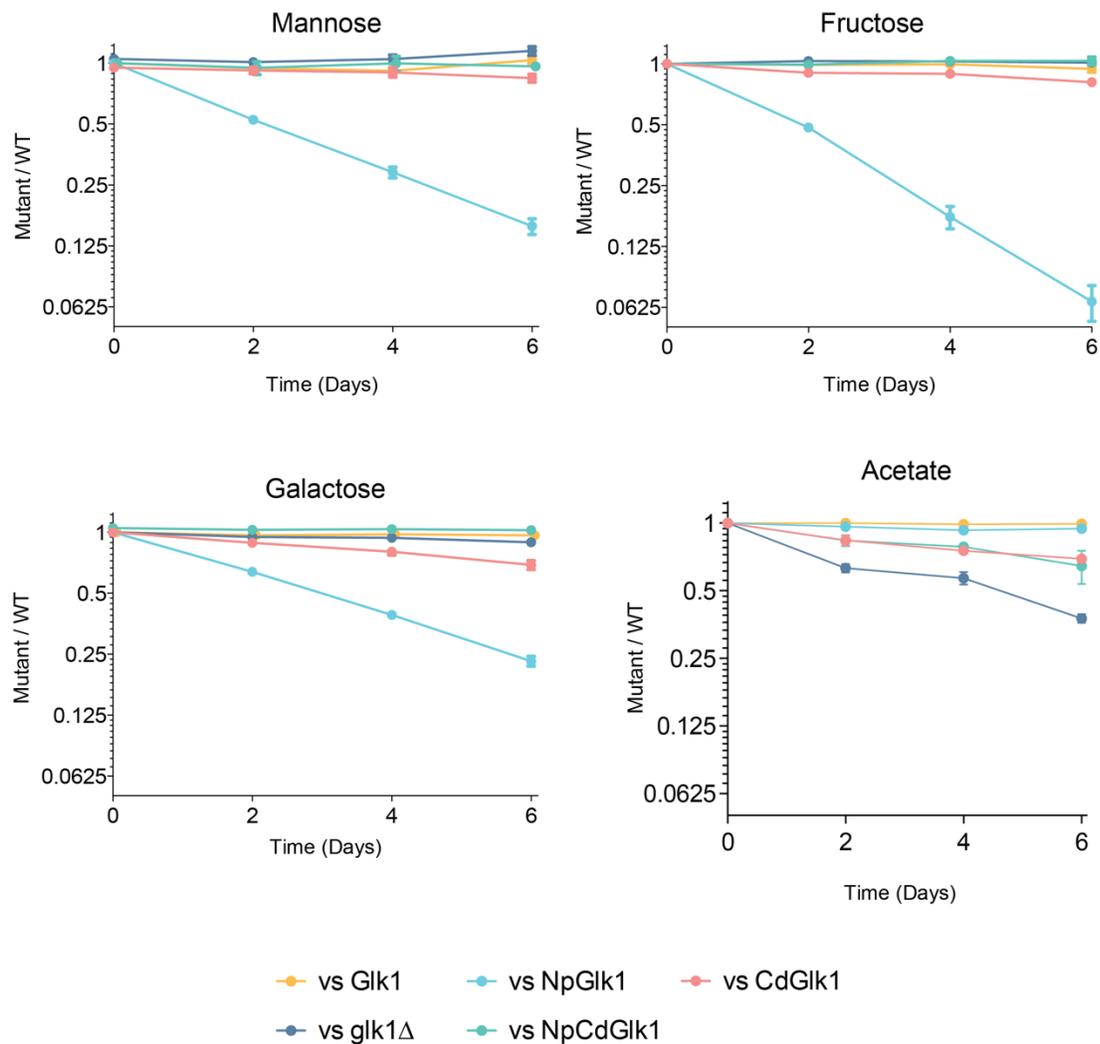


Fig. S20 - NonPol-Glk1 cells have growth defects in a variety of sugars, but not on other carbon sources.

Wild-type W303 labeled with mCherry were grown to saturation and back-diluted every 48 hours in a mixed culture with green labeled W303 (wild-type, *glk1Δ*, NonPol-Glk1, NonPolCatDead-Glk1, CatDead-Glk1) in CSM-Mannose (*top-left*), CSM-Fructose (*top-right*), CSM-Galactose (*bottom-left*), or CSM-Acetate (*bottom right*). The relative proportion of the strains were measured after each dilution by flow cytometry. NonPolGlk1 cells showed reduced fitness when grown on all sugars tested. Cells lacking Glk1 activity (*glk1Δ*, CatDeadGlk1, NonPolCatDeadGlk1) had reduced fitness when grown with acetate as the carbon source. Mean \pm SD (n=5).

Table S1: Crystallography Statistics

| | Glk1 |
|-------------------------------------|-----------------------------|
| Data Collection | |
| Wavelength (Å) | 0.9793 |
| Resolution Range (Å) | 155.8 - 3.59 (3.718 - 3.59) |
| Space Group | P 43 21 2 |
| Unit Cell (a,b,c) | 174.5, 174.5, 323.9 |
| Unit Cell (α,β,γ) | 90, 90, 90 |
| Number of Crystals | 1 |
| Total Reflections | 122,662 (12,052) |
| Unique Reflections | 61,332 (6,026) |
| Redundancy | 2.0 (2.0) |
| Completeness (%) | 99.97 (99.95) |
| Mean I/ σ (I) | 8.28 (1.56) |
| R-merge | 0.100 (0.4831) |
| R-meas | 0.142 (0.6832) |
| R-pim | 0.100 (0.4831) |
| CC 1/2 | 0.988 (0.638) |
| Refinement | |
| Resolution Range (Å) | 155.8 - 3.59 (3.718 - 3.59) |
| R-work | 0.265 (0.336) |
| R-free | 0.300 (0.357) |
| Number of Atoms | 22,953 |
| Reflections Used | 61,332 (6,025) |
| Protein Atoms | 22,888 |
| Ligand Atoms | 65 |
| Protein Residues | 2,944 |
| Ramachandran Plot | |
| Favored (%) | 98.73 |
| Allowed (%) | 1.27 |
| Outliers (%) | 0.0 |
| RMS (bonds) | 0.004 |
| RMS (angles) | 1.47 |
| Wilson B-factor | 91 |
| Average B-factor | 90 |
| Protein B-factor | 90 |
| Ligands B-factor | 76 |
| Number of TLS Groups | 20 |

Table S2: CryoEM Statistics

| | Glk1 filament (EMD-20309, PDB 6PDT) |
|---|--|
| Data collection | |
| Electron microscope | Titan Krios |
| Voltage (kV) | 300 |
| Electron detector | K2 summit |
| Exposure time (s) | 10 |
| Total electron exposure (e ⁻ /Å ²) | 90 |
| Magnification (nominal) | 130,000X |
| Super-resolution pixel size (Å) | 0.525 |
| Frames collected/movie | 50 |
| Energy filter slit width (eV) | 20 |
| Automation software | Leginon |
| Micrographs collected | 1184 |
| Defocus range (μM) | -0.8 to -2.5 |
| Reconstruction | |
| Pixel size (Å) | 1.05 |
| Particles extracted | 234,882 |
| 3D Refinement package | Relion |
| Point group symmetry | D1 |
| Refine helical symmetry | 120.4°, 60.1Å |
| Particles in final reconstruction | 56,778 |
| Relion estimated accuracy rotations | 1.945 |
| Relion estimated accuracy translations | 0.702 |
| Unmasked resolution (0.5 FSC) (Å) | 4.2 |
| Unmasked resolution (0.143 FSC) (Å) | 3.9 |
| Masked resolution (0.5 FSC) (Å) | 4.2 |
| Masked resolution (0.143 FSC) (Å) | 3.8 |
| Local resolution range (Å) | 3.7-4.9 |
| B-factor for sharpening (Å ²) | -117 |
| Model composition | |
| Protein residues | 500 |
| Ligands | ATP, glucose, Mg |
| Validation | |
| Clashscore | 1.72 |
| Poor rotamers | 0 |
| CC | 0.66 |
| RMSZ bond lengths | 1.18 |
| Bond lengths Z-score > 2 (%) | 0.6 |
| RMSZ bond angles | 1.04 |
| Bond angles Z-score > 2 (%) | 0.2 |
| Molprobity score | 0.99 |
| Clashscore | 1.7 |
| C-beta deviations | 0 |
| EMRinger score | 1.7 |
| CaBLAM outliers (%) | 2.20 |
| Ramachandran plot | |
| Favored (%) | 98 |
| Allowed (%) | 2 |
| Outliers (%) | 0 |

Table S3: Table of negative log e-values for the pairwise comparison of the HMM for each protein family in the Actin ATPase clan. A high-resolution version of this table is in supplementary file S2.

| | Actn | Heb | DhwK/Hsp70 | FuA | HM | PuPDS2A | SLA | DDR | NrADBP/DFP | HPC200A | DFP146A | Amk | Ret_Kinase | Grp_Medusa | gH2L2/Grp | FGCY | Hexokinase | Glucokinase | RK | Asc_Kinase | Pep_M22 | Carbon_Tans | Hydat | T25P | Hc_CoA_rod |
|-------------|---------|---------|------------|---------|---------|---------|---------|--------|------------|---------|---------|--------|------------|------------|-----------|---------|------------|-------------|--------|------------|---------|-------------|--------|---------|------------|
| Actn | 171.133 | 34.443 | 23.817 | 21.024 | 15.53 | 12.455 | 10.637 | 6.998 | 6.592 | 7.543 | 5.909 | 5.915 | 5.006 | 4.999 | 4.768 | 5.185 | 4.962 | 3.912 | 4.605 | 4.51 | 3.507 | 2.847 | 2.04 | 1.909 | 1.47 |
| Heb | 36.312 | 142.018 | 87.162 | 90.251 | 38.36 | 28.101 | 25.719 | 26.187 | 13.828 | 13.553 | 6.571 | 8.623 | 5.404 | 8.409 | 5.133 | 13.283 | 5.843 | 6.502 | 5.512 | 4.423 | 3.622 | 4.744 | 6.119 | 2.705 | 1.309 |
| DhwK/Hsp70 | 24.798 | 85.87 | 233.878 | 41.184 | 28.482 | 23.899 | 16.68 | 17.728 | 12.209 | 11.218 | 4.075 | 7.849 | 5.779 | 9.283 | 5.776 | 12.94 | 6.32 | 4.816 | 5.404 | 3.352 | 4.423 | 5.39 | 5.011 | 1.627 | 1.129 |
| FuA | 22.284 | 42.199 | 46.859 | 100.028 | 97.065 | 23.739 | 18.148 | 18.722 | 14.626 | 14.732 | 4.854 | 6.68 | 9.362 | 7.094 | 6.32 | 9.657 | 5.913 | 5.279 | 4.51 | 3.3 | 3.853 | 2.976 | 4.075 | 11.206 | 2.04 |
| HM | 15.934 | 36.068 | 26.471 | 100.783 | 146.724 | 17.708 | 9.23 | 18.441 | 12.88 | 13.72 | 4.618 | 10.127 | 6.119 | 7.154 | 4.343 | 8.422 | 9.35 | 7.07 | 5.221 | 3.507 | 4.343 | 2.551 | 3.244 | 27.867 | 1.386 |
| PuPDS2A | 12.717 | 27.846 | 24.264 | 25.233 | 18.873 | 133.288 | 14.592 | 13.936 | 10.925 | 11.107 | 4.343 | 9.361 | 6.32 | 9.272 | 5.15 | 6.87 | 4.249 | 4.343 | 4.51 | 4.675 | 4.722 | 4.791 | 5.279 | 0.236 | 1.386 |
| SLA | 9.987 | 22.42 | 18.118 | 17.791 | 11.251 | 11.33 | 189.137 | 9.327 | 13.41 | 18.722 | 4.819 | 4.615 | 2.642 | 9.21 | 3.817 | 8.805 | 2.267 | 3.381 | 4.343 | 10.212 | 3.863 | 2.876 | 4.51 | 2.513 | 2.917 |
| DDR | 6.315 | 71.894 | 17.302 | 22.271 | 13.754 | 13.224 | 12.34 | 90.147 | 6.501 | 13.936 | 1.51 | 3.612 | 6.264 | 9.751 | 5.119 | 7.775 | 4.343 | 5.911 | 5.199 | 2.524 | 2.94 | 4.343 | 4.605 | 0.811 | 2.64 |
| NrADBP/DFP | 7.789 | 12.943 | 11.884 | 12.94 | 10.713 | 9.485 | 11.959 | 5.279 | 296.34 | 7.236 | 4.678 | 12.424 | 3.863 | 8.874 | 3.016 | 14.201 | 3.689 | 5.139 | 7.506 | 5.221 | 10.871 | 10.483 | 3.817 | 0.511 | 18.777 |
| HPC200A | 7.562 | 13.014 | 10.925 | 14.654 | 14.002 | 9.485 | 18.965 | 14.509 | 7.339 | 280.883 | 2.986 | 2.84 | 2.501 | 6.725 | 22.82 | 7.849 | 4.343 | 3.912 | 2.919 | 4.2 | 1.05 | 1.661 | 2.207 | 1.347 | 3.507 |
| DFP146A | 4.264 | 5.843 | 4.934 | 4.095 | 4.125 | 4.656 | 3.507 | 1.897 | 1.547 | 3.772 | 296.34 | 3.817 | 5.185 | 2.207 | 0.4 | 2.293 | 2.782 | 2.614 | 8.079 | 11.418 | 0.988 | 1.661 | 2.303 | 1.897 | 1.386 |
| Amk | 6.032 | 8.079 | 7.354 | 8.468 | 9.441 | 9.111 | 5.714 | 3.324 | 12.148 | 2.207 | 3.863 | 293.33 | 3.347 | 7.749 | 2.802 | 11.652 | 2.919 | 2.305 | 5.655 | 4.613 | 7.581 | 4.343 | 0.315 | 1.679 | 4.2 |
| Ret_Kinase | 5.884 | 5.615 | 6.177 | 5.952 | 5.745 | 5.745 | 4.605 | 5.724 | 5.051 | 4.115 | 2.847 | 2.986 | 156.863 | 8.335 | 4.343 | 9.457 | 5.684 | 7.118 | 4.017 | 7.25 | 1.204 | 1.897 | 1.772 | 0.386 | 2.12 |
| Grp_Medusa | 5.827 | 9.028 | 8.948 | 8.079 | 6.438 | 8.517 | 7.339 | 10.059 | 11.564 | 7.024 | 1.643 | 2.718 | 8.168 | 313.132 | 5.714 | 11.418 | 5.38 | 7.775 | 5.038 | 6.571 | 3.853 | 0.842 | 15.713 | 0.811 | 1.813 |
| gH2L2/Grp | 4.962 | 4.867 | 4.841 | 4.867 | 3.712 | 3.12 | 4.98 | 5.521 | 3.058 | 24.355 | 1.139 | 2.93 | 2.587 | 3.027 | 389.83 | 5.38 | 6.075 | 4.125 | 2.107 | 4.249 | 5.565 | 0.462 | 0.328 | 1.609 | 1.627 |
| FGCY | 4.744 | 13.553 | 13.978 | 11.043 | 9.21 | 6.075 | 8.377 | 5.473 | 15.938 | 9.294 | 6.511 | 13.174 | 7.524 | 9.887 | 5.147 | 211.306 | 8.005 | 6.571 | 12.289 | 6.735 | 8.079 | 8.874 | 4.343 | 0.274 | 1.027 |
| Hexokinase | 4.836 | 6.166 | 6.075 | 7.024 | 9.79 | 4.343 | 4.2 | 4.2 | 4.239 | 5.449 | 2.384 | 2.12 | 5.279 | 3.382 | 5.891 | 10.724 | 281.119 | 18.489 | 16.281 | 4.249 | 0.654 | 2.847 | 1.661 | 0.386 | 1.05 |
| Glucokinase | 4.895 | 7.002 | 6.371 | 5.426 | 7.024 | 4.733 | 4.115 | 3.863 | 6.075 | 5.521 | 1.609 | 1.609 | 7.017 | 9.481 | 5.14 | 8.948 | 20.518 | 208.254 | 30.29 | 7.929 | 0.734 | 1.609 | 3.983 | 0.938 | 0.713 |
| RK | 6.12 | 5.288 | 4.2 | 5.229 | 5.484 | 4.135 | 4.017 | 5.071 | 7.621 | 2.807 | 8.874 | 5.497 | 9.298 | 4.823 | 1.813 | 12.717 | 17.651 | 29.865 | 105.45 | 11.475 | 2.621 | 1.966 | 2.865 | 1.105 | 1.609 |
| Asc_Kinase | 4.943 | 4.51 | 3.612 | 4.017 | 3.101 | 5.655 | 10.82 | 2.04 | 1.809 | 5.426 | 12.405 | 5.531 | 5.167 | 4.166 | 5.067 | 6.075 | 4.934 | 8.568 | 11.761 | 201.042 | 2.703 | 3.244 | 0.261 | 1.109 | 1.079 |
| Pep_M22 | 4.017 | 1.85 | 4.2 | 1.079 | 3.016 | 3.912 | 3.324 | 1.659 | 11.533 | 1.427 | 1.204 | 6.377 | 1.713 | 1.833 | 0.38 | 7.419 | 1.171 | 0.58 | 2.996 | 3.507 | 219.502 | 10.127 | 0.223 | 1.204 | 1.897 |
| Carbon_Tans | 1.058 | 3.418 | 5.889 | 4.268 | 2.9 | 4.744 | 1.017 | 3.71 | 8.848 | 1.772 | 1.617 | 4.485 | 2.457 | 1.427 | 0.371 | 8.74 | 2.264 | 2.817 | 1.167 | 1.642 | 10.962 | 34.791 | 0.261 | 0.944 | 2.817 |
| Hydat | 2.749 | 7.143 | 4.32 | 4.976 | 4.143 | 6.166 | 4.956 | 5.288 | 5.714 | 3.111 | 1.218 | 0.58 | 2.404 | 16.946 | 0.944 | 6.37 | 3.077 | 5.205 | 4.149 | 1.273 | 0.948 | 1.661 | 286.34 | 0.842 | 1.109 |
| T25P | 1.309 | 2.207 | 1.022 | 11.251 | 26.172 | 0.188 | 2.207 | 0.588 | 0.371 | 1.347 | 1.273 | 1.199 | 0.274 | 0.261 | 0.835 | 0.288 | 0.616 | 1.05 | 1.139 | 0.844 | 1.079 | 0.545 | 2.303 | 158.116 | 0.811 |
| Hc_CoA_rod | 1.022 | 1.309 | 0.511 | 1.772 | 1.735 | 1.171 | 2.749 | 1.966 | 20.03 | 3.963 | 1.079 | 3.194 | 1.772 | 1.427 | 1.109 | 0.673 | 0.916 | 0.462 | 1.609 | 1.109 | 1.833 | 2.951 | 0.301 | 1.204 | 201.018 |

Table S4. Strains and Plasmids Used in This Study

| Strain | Genotype | Source |
|--------|---|-------------------|
| yPS003 | W303 (ura3 ade2-1 his3-11,15 leu2-3,112 trp1-1 Mata BUD4 GLK1-msfGFP::spHIS5) | <i>This Study</i> |
| yPS031 | W303 (ura3 ade2-1 mCherry::HIS leu2-3,112 trp1-1 Mata BUD4) | <i>This Study</i> |
| yPS033 | W303 (ura3 ade2-1 Citrine::HIS leu2-3,112 trp1-1 Mata BUD4) | <i>This Study</i> |
| yPS041 | W303 (ura3 ade2-1 Citrine::HIS leu2-3,112 trp1-1 Mata BUD4 glk1Δ::HPH) | <i>This Study</i> |
| yPS106 | W303 (ura3 ade2-1 his3-11,15 leu2-3,112 trp1-1 Mata BUD4 Glk1(F3S)) | <i>This Study</i> |
| yPS108 | W303 (ura3 ade2-1 his3-11,15 leu2-3,112 trp1-1 Mata BUD4 GLK1(F3S,K182A)) | <i>This Study</i> |
| yPS109 | W303 (ura3 ade2-1 his3-11,15 leu2-3,112 trp1-1 Mata BUD4 Glk1(K182A)) | <i>This Study</i> |
| yPS110 | W303 (ura3 ade2-1 his3-11,15 leu2-3,112 trp1-1 Mata BUD4 Glk1(F3S)-msfGFP::URA) | <i>This Study</i> |
| yPS111 | W303 (ura3 ade2-1 his3-11,15 leu2-3,112 trp1-1 Mata BUD4 GLK1(F3S,K182A)-msfGFP::URA) | <i>This Study</i> |
| yPS112 | W303 (ura3 ade2-1 his3-11,15 leu2-3,112 trp1-1 Mata BUD4 Glk1(K182A)-msfGFP::URA) | <i>This Study</i> |
| yPS113 | W303 (ura3 ade2-1 Citrine::HIS leu2-3,112 trp1-1 Mata BUD4 Glk1(F3S)) | <i>This Study</i> |
| yPS116 | W303 (ura3 ade2-1 Citrine::HIS leu2-3,112 trp1-1 Mata BUD4 Glk1(K182A)) | <i>This Study</i> |
| yPS117 | W303 (ura3 ade2-1 Citrine::HIS leu2-3,112 trp1-1 Mata BUD4 Glk1(F3S,K182A)) | <i>This Study</i> |

| Plasmid | Description | Source |
|-----------------|---|-------------------|
| pSUMO-Glk1 | his6-SUMO tagged <i>S. cerevisiae</i> Glucokinase in T7 expression vector (AMP) | <i>This Study</i> |
| pSUMO-caglGlk1 | his6-SUMO tagged <i>C. glabrata</i> Glucokinase in T7 expression vector (AMP) | <i>This Study</i> |
| pSUMO-caalGlk1 | his6-SUMO tagged <i>C. albicans</i> Glucokinase in T7 expression vector (AMP) | <i>This Study</i> |
| pSUMO-scpoHxk1 | his6-SUMO tagged <i>S. pombe</i> Glucokinase in T7 expression vector (AMP) | <i>This Study</i> |
| pSUMO-nacaGlk1 | his6-SUMO tagged <i>N. castellii</i> Glucokinase in T7 expression vector (AMP) | <i>This Study</i> |
| pSUMO-lakiGlk1 | his6-SUMO tagged <i>L. kluyveri</i> Glucokinase in T7 expression vector (AMP) | <i>This Study</i> |
| pSUMO-vapoGlk1a | his6-SUMO tagged <i>V. polysporus</i> Glucokinase-1 in T7 expression vector (AMP) | <i>This Study</i> |
| pSUMO-vapoGlk1b | his6-SUMO tagged <i>V. polysporus</i> Glucokinase-2 in T7 expression vector (AMP) | <i>This Study</i> |
| pSUMO-kliaGlk1 | his6-SUMO tagged <i>K. lactis</i> Glucokinase in T7 expression vector (AMP) | <i>This Study</i> |
| pSUMO-ergoGlk1 | his6-SUMO tagged <i>E. gossypii</i> Glucokinase in T7 expression vector (AMP) | <i>This Study</i> |
| pSUMO-Hxk1 | his6-SUMO tagged <i>S. cerevisiae</i> Hexokinase-1 in T7 expression vector (AMP) | <i>This Study</i> |
| pSUMO-Hxk2 | his6-SUMO tagged <i>S. cerevisiae</i> Hexokinase-2 in T7 expression vector (AMP) | <i>This Study</i> |
| pSUMO-scpoHxk2 | his6-SUMO tagged <i>S. pombe</i> Hexokinase in T7 expression vector (AMP) | <i>This Study</i> |
| pSUMO-yaliGlk1 | his6-SUMO tagged <i>Y. lipolytica</i> Glucokinase in T7 expression vector (AMP) | <i>This Study</i> |
| pSUMO-dehaGlk1 | his6-SUMO tagged <i>D. hansenii</i> Glucokinase in T7 expression vector (AMP) | <i>This Study</i> |
| pSUMO-hauvGlk1 | his6-SUMO tagged <i>H. uvarum</i> Glucokinase in T7 expression vector (AMP) | <i>This Study</i> |
| pSUMO-asruGlk1 | his6-SUMO tagged <i>A. rubescens</i> Glucokinase in T7 expression vector (AMP) | <i>This Study</i> |

Movie S1: Glk1-GFP Polymerization is Induced by Glucose. Glk1-GFP cells grown to stationary phase were loaded into a flow cell. At the start of the movie, CSM-glucose medium is flowed over the cells, inducing Glk1 polymerization. The movie is a maximum intensity projection of a confocal z-stack. Images were taken at 5-second intervals. Movie begins 20 seconds before glucose addition, which occurs at 0 seconds.

Movie S2: Glk1-GFP Depolymerizes When Glucose is Removed. Glk1-GFP cells grown to saturation were loaded into a flow cell and washed into glucose-containing medium. At the start of the movie, glucose is washed out by washing the cells into CSM medium with no carbon source. The movie is a single confocal slice with continuous capture. Images were taken at 100 ms intervals. Movie begins 10 seconds before glucose withdrawal, which occurs at 0 seconds.